Plasma Jets in a Turbulent Channel Flow

Crossflow-oscillating plasma jets in a turbulent channel flow

F. M. Ricci, E. Amico, G. Cafiero, G. Iuso and J. Serpieri

Abstract To investigate the effect of friction drag manipulation, an array of plasma actuators was designed to induce a wall jet oscillating along the opposite crossflow directions. Besides, steady mono-directional and bi-directional forcing were performed too. Pressure measurements and optical flow diagnostics were deployed to inspect the effect of the operated actuation on a fully-developed turbulent flow.

1 Introduction

In recent efforts, plasma actuators (PAs) have been considered as plausible flow actuators to induce a Stokes-like wall flow, similar to what caused by oscillating the flow-exposed surfaces along the crossflow direction, and capable of reducing the friction drag exerted by turbulent flows (e.g. [1, 2, 3, 4]). The interest they collected is motivated by their simpler embodiment compared to mechanical, pneumatic or piezo-electric devices (e.g. [5, 6, 7, 8, 9]). Nevertheless, the flow control effect that they induce differs from the more studied and understood strategies based on displacing the flow exposed surfaces and deserves more investigations. This study is motivated by this need.

2 Experimental setup

The experimental campaign took place in a channel flow facility (0.42 m x 0.035 m x 10 m, in width, height h and length), operated at the friction Reynolds numbers of

F. M. Ricci, E. Amico, G. Cafiero, G. Iuso and J. Serpieri*
Department of Mechanical and Aerospace Engineering, Politecnico di Torino,
Corso Duca degli Abruzzi, 24, 10129, Turin, Italy,
*Corresponding author e-mail: Jacopo.Serpieri@me.com

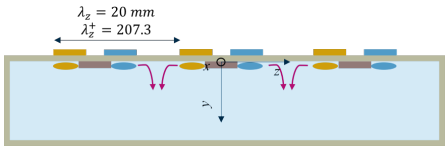

Fig. 1: Schematics of the setup as seen in a crossflow plane (not to scale): actuators spacing (λ_z, λ_z^+), operated electrodes (yellow and blue rectangles), exposed electrodes (brown rectangles), plasma discharges (oval shapes colored as the related HV electrodes), colliding plasma jets (magenta arrows).

$Re_\tau = \frac{u_\tau h/2}{\nu} = 190$ (where u_τ is the friction velocity and ν the kinematic viscosity). Pressure taps every 0.20 m along the streamwise direction are installed in the channel walls. These pressure taps were connected to a piezo-resistive pressure transducer (*DSA*) operated at 20 Hz and set to acquire for 200 s for statistical significance of the temporal averages.

The flow actuator hereby considered featured an array of six dielectric barrier discharge (DBD) PAs with the electrodes aligned with and extending 600 mm along the streamwise direction. The PAs considered 0.5 mm thick polyethylene terephthalate sheets as the dielectric layer. The electrodes were made with 0.35 mm thick copper tape and the isolation of the encapsulated electrodes was guaranteed by multiple layers of *Kapton* tape. Every actuator featured one exposed electrode connected to the ground and two encapsulated electrodes, one per side of the exposed electrode, each connected to a high voltage (HV) source. The latter were four *GBS Elektronik Minipuls 4* supplied with a 7 kHz signal and set to deliver a sinusoidal signal of peak-to-peak amplitude of 8 kV. A schematic of the actuator installed in the channel is shown in figure 1, together with the coordinates system used in this study: x is the streamwise direction, while y and z are the wall normal and the crossflow ones, respectively. x originates at the actuator upstream edge, y at the wall and z at the channel center-line. The velocity components along these directions are denoted with u, v, w, respectively. Reynolds decomposition will be considered: $[u(t), v(t), w(t)] = [U, V, W] + [u'(t), v'(t), w'(t)]$, where t is time and upper case letters and overlines, in the remainder, imply time-averages.

According to the chosen actuation strategy, the HV signals were opportunely modulated. A schematic of the voltage-modulation effect can be extracted from figure 1. For the actuation strategy aiming at replicating the oscillating wall forcing, either the yellow or blue actuators were operated at the same instant and each set was operated for 50 % of the modulation cycle. Consequently, for this case, either the yellow or blue colored plasma discharges took place. The modulation frequency was set to meet the literature-deemed-optimal non-dimensional period of $T^+ = 100$ (where the + labeled quantities are non-dimensionalised with inner-layer scales) (see [6]). When instead the steady monodirectional forcing is considered, only the blue electrodes were constantly operated, therefore leading only to the blue-colored plasma discharges. This case is referred to as $w_{PAs} > 0$. Finally, the case where both

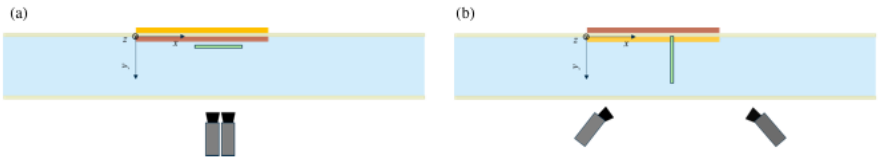

Fig. 2: Schematics side view of the PIV (a) and SPIV (b) setups (not to scale): channel and actuators shown as in figure 1, laser plane (light green) and cameras (grey shapes).

the electrodes sets were constantly operated was also considered. In these conditions, the plasma-induced jets from both the electrodes sets collided halfway and generated upwash (i.e. $y \rightarrow h/2$) fluid motions (see [7, 10]). This is also shown in figure 1 with the magenta arrows, together with the crossflow spacing of the actuators: $\lambda_z = 20$ mm ($\lambda_z^+ = 207.30$ for the reference flow; i.e. about twice the average streaks' spacing).

Two different optical flow diagnostics experiments were set up: a xz plane PIV setup (see figure **??**) and a yz plane stereographic PIV (SPIV) setup (see figure **??**). Both setups consisted of two *Andor Zyla* sCMOS cameras (5.5 Mpx, 16 bits) and a *Litron* double cavity laser (200 mJ/pulse, 15 Hz maximum repetition rate). The cameras were equipped with *Tokina* 100 mm macro lens with green filters and, for the SPIV setup, with Scheimpflug-condition adapters from *LaVision*. The system synchronization was guaranteed by a *National Instrument PCI-6602* board. The acquisition frequency was 15 Hz and a total of 1000 image pairs was acquired.

The PIV setup featured the two cameras placed one next to the other along the streamwise direction such to image a total field of view (FOV) extending 111.90 mm x 48.10 mm along the $x-z$ directions. This corresponds, in non-dimensional units, to 1550 x 497.40 along x^+-z^+. The illuminated plane was set at $y = 5$ mm ($y^+ = 51.82$). The final velocimetry resolution was 3.67 vectors/mm, i.e. 0.35 vectors per viscous length scale. The thickness of the laser sheet was set to ≈ 0.5 mm using light knives.

The SPIV setup investigated a domain extending 29.50 mm x 22 mm along z and y, thus 305.70 x 227.98 along $z^+ - y^+$. The plane was set at $x = 546$ mm ($x^+ = 5.67\,10^3$) from the actuator upstream edge. The velocimetry resolution was 9.26 vectors/mm (0.89 vectors per viscous length scale). The thickness of the laser sheet was increased to ≈ 1.5 mm to guarantee a good dynamic range.

3 Results and discussion

The effect of the performed flow actuation measured by the differential pressure transducer shows rather similar behaviors for all the three actuation strategies compared to the reference unforced flow. First, at the upstream stations, all the actuated flows showed, for the same fan speed, a higher level of pressure. This could be explained as a flow-blockage effect induced by the plasma jets. Then, moving along

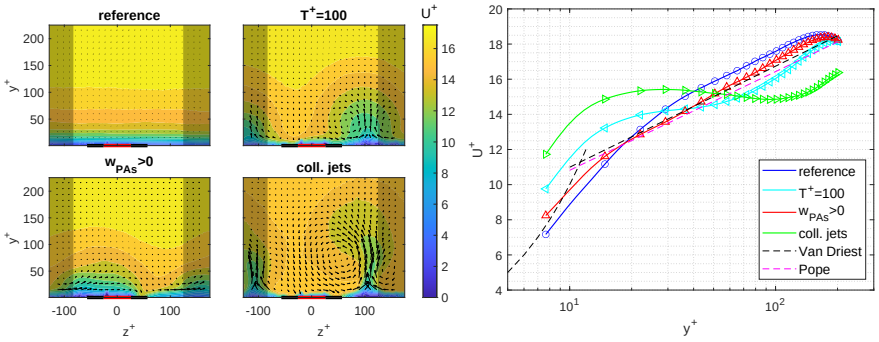

Fig. 3: SPIV time-averaged fields: (a) $V - W$ fields (vectors) on U contours; 1:10 vectors shown (arbitrary length); exposed electrodes (red line), HV electrodes (black lines); (b) λ_z-averaged U profiles (un-shaded areas of (a)); 1:7 measurements shown; black dashed line from [11]; red dashed line from [12].

the streamwise direction, as the flow undergoes actuation, the slope of the differential pressure decreased whereas, moving downstream of the actuation region, the slope recovered to the unforced value (see also [4]). Such behaviour of the pressure trend is thought to be initially caused by the downwash ($y \rightarrow 0$) motions of higher-momentum fluid needed to comply with mass continuity and the plasma-jets-induced crosswise momentum. On the other side, at more downstream stations, the beneficial effect of the performed actuation is likely overcoming this negative (drag enhancing) effect and a lower pressure drop was observed for the actuated flow cases.

The SPIV setup allows to inspect the effect of the different actuation strategies on cross-stream planes. The time-averaged velocity fields are shown in figure 3a. The fields are made non dimensional using the reference flow friction velocity u_τ. While, the reference flow features a crosswise-uniform streamwise velocity field with non-appreciable in-plane velocity components, all the forced flows present strong in-plane motions with related crosswise modulations of the streamwise velocity component. In particular, the $T^+ = 100$ case, shows time-averaged wall normal fluid motions between the actuators ($z^+ \approx \pm 103$). At the same time, a downwash sets over the exposed electrode, or at slightly more negative z positions (the reason of this misalignment might be due to small differences in the induced jets' strength). This flow scenario appears similar to the "colliding jets" case where both electrodes' sets are constantly operated; albeit this appears somewhat milder for the $T^+ = 100$ case. The similarity between these two fields suggests that for the considered actuators' spacing and jets strength, the induced flow does not fully resemble, for the crossflow-oscillating case, the Stokes-like flow where a wall layer of crosswise velocity was desired. The $w_{PAs} > 0$ case also shows a crosswise modulation but with weaker wall-normal fluid motions.

Wall-normal profiles, averaged along one λ_z, of streamwise velocity are shown in figure 3b together with the [12, 11] law of the wall profiles. While for the reference case, the measured values nicely lay on the logarithmic distribution, all the forced

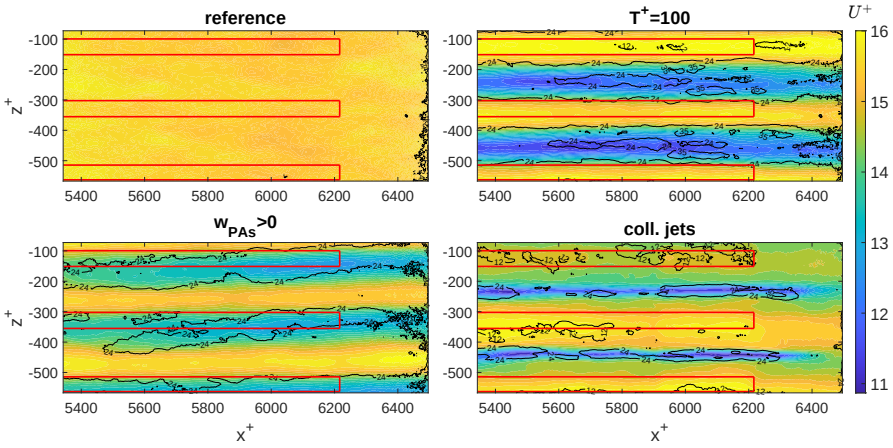

Fig. 4: U^+ (colors) and $\overline{u'^{2+}}$ (isolines) fields and PAs' exposed electrodes (red lines).

flow curves feature more non-homogeneous distributions. Namely, the log-layer velocities attain to lower values compared to the reference flow; whereas, the buffer-layer appears inflated by the performed flow actuation.

The velocity fields measured by the PIV setup are also useful to describe the effect of the plasma jets. The time-averaged U^+ fields are presented in figure 4: a strong modulation from the performed actuation is here evident too, especially for the $T^+ = 100$ and the "colliding jets" cases. The $w_{PAs} > 0$ field shows the velocity isolines tilted towards larger z as a consequence of the monodirectional actuation. The standard deviation $\overline{u'^{2+}}$ velocity fields are shown too in figure 4. While for the $T^+ = 100$ case, two larger $\overline{u'^{2+}}$ regions are evident, due to the temporal modulation of the induced motions, the $w_{PAs} > 0$ flow features more compact regions of larger $\overline{u'^{2+}}$, related to the shears induced by the strong upwash motion between the actuators.

The occurrence and strength of low-speed streaks (LSS) of streamwise velocity are directly connected to larger skin friction events. As such, the LSS features are analysed extracting connected regions of $u' < 0$, extending in the streamwise direction for at least 100 viscous length scales. The velocity fields are then conditionally averaged to derive LSS statistical features. These are shown in figure 5. Figure 5a shows that the $T^+ = 100$ and $w_{PAs} > 0$ forcing reduce, at the measurement plane, the velocity deficit within the LSS. Figure 5b reveals that the wall-normal vorticity ω'_y within the LSS is much reduced by all the considered forcing. The flow actuation increases the probability (pdf) of larger streaks' length L_s^+ (figure 5c) whereas, has milder effects on their average width W_s^+ (figure 5d).

The preliminary results hereby presented show strong effects from the performed actuation on the operated time-averaged flow as well as on the coherent turbulent structures. These will be analysed and discussed in future studies.

Acknowledgements The authors are grateful to T. Astarita for the (S)PIV software.

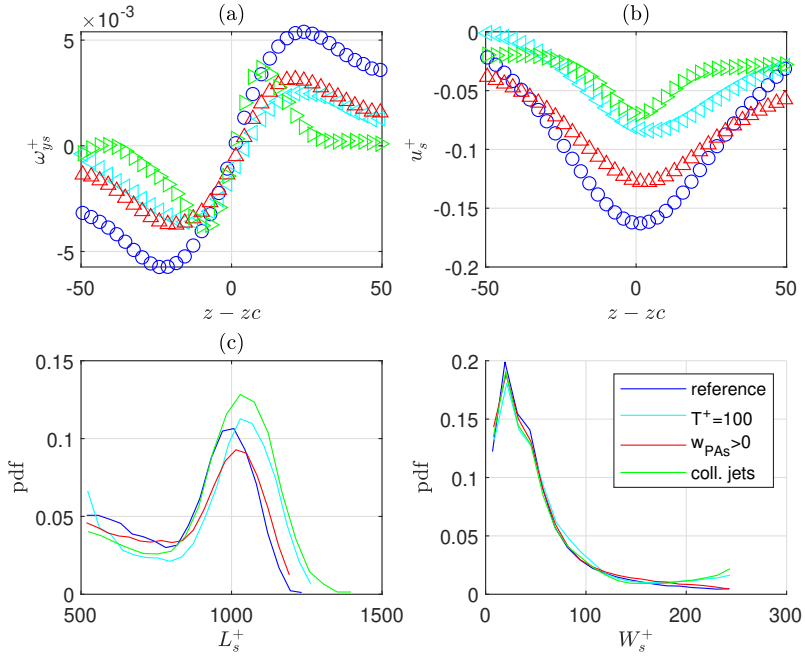

Fig. 5: LSS features for the considered flow cases: ${\omega'_{ys}}^+$ (a); ${u'_s}^+$ (b); pdf of L^+_s (c) and pdf of W^+_s (d); z_c is the LSS center along z.

References

1. K.S. Choi, T. Jukes, R. Whalley, Philosophical Transactions of the Royal Society A: Mathematical, Physical and Engineering Sciences **369**(1940), 1443 (2011). DOI 10.1098/RSTA.2010.0362
2. R.D. Whalley, K.S. Choi, Experiments in Fluids **55**(8) (2014). DOI 10.1007/S00348-014-1796-3
3. M.T. Hehner, D. Gatti, P. Mattern, M. Kotsonis, J. Kriegseis, AIAA Journal **59**(2), 763 (2021). DOI 10.2514/1.J059802
4. J. Serpieri, M.T. Hehner, J. Kriegseis, Flow, Turbulence and Combustion (2023). DOI 10.1007/s10494-023-00463-w
5. G.M. Di Cicca, G. Iuso, P.G. Spazzini, M. Onorato, Journal of Fluid Mechanics (2002). DOI 10.1017/S002211200200157X
6. G.E. Karniadakis, K.S. Choi, Annual Review of Fluid Mechanics **35**, 45 (2003). DOI 10.1146/annurev.fluid.35.101101.161213
7. G. Iuso, G.M. Di Cicca, Journal of Turbulence (2009). DOI 10.1080/14685240601110088
8. F. Auteri, A. Baron, M. Belan, G. Campanardi, M. Quadrio, Physics of Fluids **22**(11) (2010). DOI 10.1063/1.3491203
9. I. Marusic, D. Chandran, A. Rouhi, M.K. Fu, D. Wine, B. Holloway, D. Chung, A.J. Smits, Nature Communications **12**(1), 1 (2021). DOI 10.1038/s41467-021-26128-8
10. X.Q. Cheng, C.W. Wong, F. Hussain, W. Schröder, Y. Zhou, Journal of Fluid Mechanics **918**, 1 (2021). DOI 10.1017/jfm.2021.311
11. E. Van Driest, Journal of the Aeronautical Sciences (1956). DOI doi:10.2514/8.3713
12. S.B. Pope, Cambridge University Press (2000)